Assignment 1
DC system steady state analysis

J. Schindler, N. Murillo, S. Matta

DC technology and systems
Supervised by Eduardo Prieto, Ferran Bohigas, Oriol Gomis

April 1, 2025

1 Introduction

This report presents the modeling and steady-state analysis of a 21-node DC microgrid incorporating real industrial and residential demand profiles, as well as distributed photovoltaic generation. The objective is to evaluate the impact of load and generation allocation, as well as grid connection configurations, on system performance. All simulations were conducted using MATLAB and GridCal, combining numerical and topological methods to assess power flow, voltage stability, and energy losses under realistic operating conditions.

2 DC Microgrid

A 21-node network structure was chosen for the project. The topology, together with the line resistances and the loads was copied from the paper [1]. In this network, there are two slack buses (1 and 21) with voltage setpoints at 1 pu and 1.05 pu. The generated power is provided solely through these slack buses. Later-on, additional generation will be added.

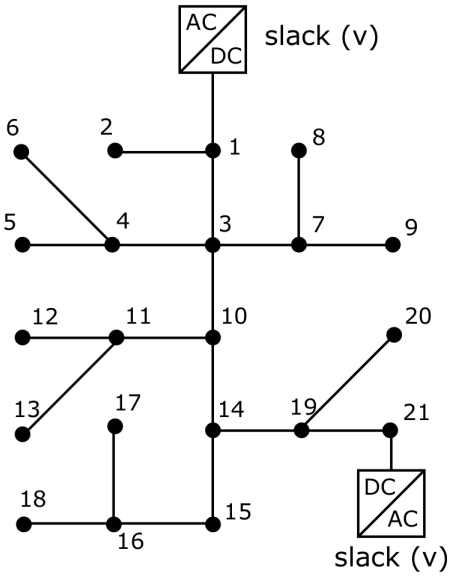

Figure 2: Microgrid Topology

From	1	2	3	4	5	6	7	8	9	10	11	12	13	14	15	16	17	18	19	19
To	2	3	4	5	6	7	8	9	10	11	12	13	14	15	16	17	18	19	20	21
Resistance [p.u.]	0.0053	0.0054	0.0054	0.0063	0.0051	0.0037	0.0079	0.0072	0.0053	0.0038	0.0079	0.0078	0.0083	0.0065	0.0064	0.0074	0.0081	0.0078	0.0084	0.0082

Table 1: Resistances

Bus	2	3	4	5	6	7	8	9	10	11	12	13	14	15	16	17	18	19	20	21
P [p.u.]	0.7	0	0.36	0.04	0.36	0	0.32	0.8	0	0.45	0.68	0.1	0	0.22	0.23	0.43	0.34	0.09	0.21	0

Table 2: Loads

3 Power Flow Calculation

The procedure of power flow calculation can be started by viewing each node as a combination of apparent power injections S_i, loads who's currents are limited by admittances Y_{ii} and interconnections to further buses through lines with impedances Y_{ij} and Y_{il} and corresponding power flows.

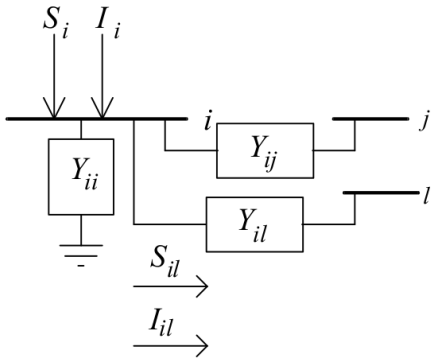

Figure 3: Node Model

The aforementioned impedances with their corresponding voltage and current relations can be formulated into a matrix expression as in equation 2. From the apparent power expression in equation 3 the non-linear nature of the problem emerges (V_i times V_k).

$$I_i = \sum_k I_{ik} \quad \xrightarrow{\text{(non) diagonal}} \quad I_{ik} = \begin{cases} Y_{ik}(V_i - V_k), & k \neq i \\ Y_{ii}V_i, & k = i \end{cases} \tag{1}$$

$$I_i = Y_{ii}V_i + \sum_{k=i,k\neq i}^{N} Y_{ik}(V_i - V_k) \quad \xrightarrow{\text{Matrix Eq.}} \quad \mathbf{I} = \mathbf{Y}_{\text{bus}}\mathbf{V} \tag{2}$$

$$S_i = V_i I_i^* = V_i \left(\sum_{k=1}^{N} Y_{ik}V_k \right)^* = V_i \sum_{k=1}^{N} Y_{ik}^* V_k^* \tag{3}$$

For AC systems, the relations get even more non-linear and common approaches for linear power flow analysis include assuming voltage levels at 1 p.u., small angular differences $cos(\Delta\Theta) \approx 1$ and $sin(\Delta\Theta) \approx \Delta\Theta$ and significantly small resistances compared to impendances to neglect conductance g_{ik}.

$$V_i = |V_i|e^{j\theta_i} \qquad \theta_{ik} = \theta_i - \theta_k \qquad y_{ik} = g_{ik} + jb_{ik} \tag{4}$$

$$S_i = \sum_{k=1}^{N} |V_i||V_k|(\cos\theta_{ik} + j\sin\theta_{ik})(g_{ik} - jb_{ik}) \tag{5}$$

$$P_i = \sum_{k=1}^{N} |V_i||V_k|(g_{ik}\cos(\theta_i - \theta_k) + b_{ik}\sin(\theta_i - \theta_k)) \tag{6}$$

3.1 Linear DC Power Flow Method

The structure of the linear DC power flow method is very similar to the linear AC power flow method. For steady-state DC power flow, the following parameters are true:

- The line reactance $X_{ser} = 0$
- The line shunts $X_{sh} = 0$
- The angle $\theta_i^{DC} = 0$
- The reactive power $Q_i^{inj,DC} = 0$

For this implementation, the power injections are assumed as known and the voltage at each bus shall be calculated. The active power injection into a bus is obtained through the power balance approach, when in- and outgoing currents (multiplied by the bus voltage) are not zero, the remaining power is the injected one. The current can be substituted by taking the difference of bus potentials and dividing by the line resistance. By applying the simplification, that all bus voltages are close to 1 pu with a small deviation v_i^{DC}, we get the linear power flow expression in equation 8.

$$P_i^{\mathrm{inj,DC}} = V_i^{\mathrm{DC}} \sum_{j=1}^{N^{\mathrm{DC}}} I_j = V_i^{\mathrm{DC}} \sum_{j=1}^{N^{\mathrm{DC}}} \frac{V_i^{\mathrm{DC}} - V_j^{\mathrm{DC}}}{R_{ij}} \quad \xleftarrow{apply} \quad V_i^{\mathrm{DC}} = 1 \text{ p.u.} + v_i^{\mathrm{DC}} \tag{7}$$

$$P_i^{\mathrm{inj,DC}} = \sum_{j=1}^{N^{\mathrm{DC}}} \frac{v_i^{\mathrm{DC}} - v_j^{\mathrm{DC}}}{R_{ij}} \quad \xrightarrow{\text{Matrix Eq.}} \quad \mathbf{v^{DC}} = (\mathbf{G'^{DC}})^{-1}\mathbf{P^{DC}} \tag{8}$$

G' is obtained by eliminating the reference bus columns and rows. The power flows in each line are then calculated using the bus voltages and the line resistances:

$$g_{ii} = \sum_{k=1}^{N} G_{ik} \qquad g_{ik} = -G_{ik} \tag{9}$$

$$P_{flow,ij} = \frac{v_j - v_i}{R_{ij}} \tag{10}$$

3.2 Non-Linear Power Flow Method

For a DC network, the following expression, as determined by Kirchhoff's laws, holds:

$$\begin{bmatrix} i_1 \\ \vdots \\ i_k \\ \vdots \\ i_n \end{bmatrix} = \begin{bmatrix} G_{11} & \dots & G_{1k} & \dots & G_{1n} \\ \vdots & \ddots & \vdots & \ddots & \vdots \\ G_{k1} & \dots & G_{kk} & \dots & G_{kn} \\ \vdots & \ddots & \vdots & \ddots & \vdots \\ G_{n1} & \dots & G_{nk} & \dots & G_{nn} \end{bmatrix} \begin{bmatrix} v_1 \\ \vdots \\ v_k \\ \vdots \\ v_n \end{bmatrix} = \mathbf{I} = \mathbf{GV}$$

where the terms v_k and i_k correspond to the nodal voltages and the net injected currents, respectively.

The net injected powers are obtained using the expression:

$$p_k = p_k^g - p_k^d = v_k \sum_{m=1}^{n} G_{km} v_m = v_k i_k$$

In DC networks, two types of nodes are modeled. On one hand, there are nodes where the voltage is known; for these nodes, it is necessary to calculate the net injected power. This type of node yields linear equations and forms a subset of linear system of equations.

The second type of node is where the net injected power is known, which implies that both the demanded power and the generated power within the node is also know, thus, the node voltage must be determined. These nodes yield nonlinear equations because voltages are multiplied, giving rise to quadratic terms. In such cases, numerical methods must be employed. Although there exists a wide range of methods in the literature, in this project the MATLAB function `fsolve` was used. To use this function, it is first necessary to create a function handler that encapsulates the information related to the model. The general structure for solving a power flow for a N-node network is presented below.

```
f1 = @(x) DC_fsolve(x, obj.G);

[x_sol, fval] = fsolve(f1, x_initial);
function y = DC_fsolve(x, G)
    % Constant voltage nodes
    y(i_1) = -v_i1 + x(i_1);
    y(i_2) = -v_i2 + x(i_2);
    % ...
    y(i_m) = -v_im + x(i_m);
    % ...

    % Constant power nodes
    y(j_1) = P_j1 + x(j_1) * x(n + j_1);
    y(j_2) = P_j2 + x(j_2) * x(n + j_2);
    % ...
    y(j_h) = P_jh + x(j_h) * x(n + j_h);
    % ...

    % Grid equations
    y(n+1:2*n) = -x(n+1:2*n)' + G * x(1:n)';
end
```

Here, n is the number of nodes, $i_1, i_2, \ldots, i_m, \ldots$ denote the nodes with known voltage, and $j_1, j_2, \ldots, j_h, \ldots$ denote the nodes with known inyected power. The term v_{im} represents the known voltage at node m and P_{jh} is the known power at node h.

The operation of `fsolve` is based on minimizing the values contained in the array y by varying the elements of the vector x, which represent the voltages and currents, using optimization methods. The adequacy of the obtained solution is verified by examining the values in the variable `fval`—these are the values of the array y when the solution x_{sol} is used. These values must be small; if large values are obtained, it implies that the power flow did not converge, likely due to voltage stability and power transfer issues.

3.3 Implementation in GridCal

The DC microgrid was set up in GridCal. Since the power base can not be adapted below 1 MW there was a change of basis for the line resistances. Other additional adjustments for the proper use of GridCal include setting the node type correctly. In our base case, there were two nodes with fixed voltage; in GridCal, this translates to configuring the node with `is slack` set to true. Additionally, for the generator connected to these nodes, it is necessary to define the V setpoint and change its configuration `is controlled` to true. The final required change, both for these generators (which represent connections to the main grid) and for the rest of the generators used in subsequent analyses, is to set the power factor value to 1. Otherwise, the program will perform calculations using reactive power, which does not make sense in DC networks.

The solver was set to use the Newton-Raphson algorithm with a tolerance of 10^{-10} a trust radius of 0.5, a maximum of iterartions of 40 and a verbosity of 0. The calculations take 30 iterations to converge to an error of $7.66 \cdot 10^{-11}$.

The network model was built in GridCal and is shown below, using all the parameters provided in [1].

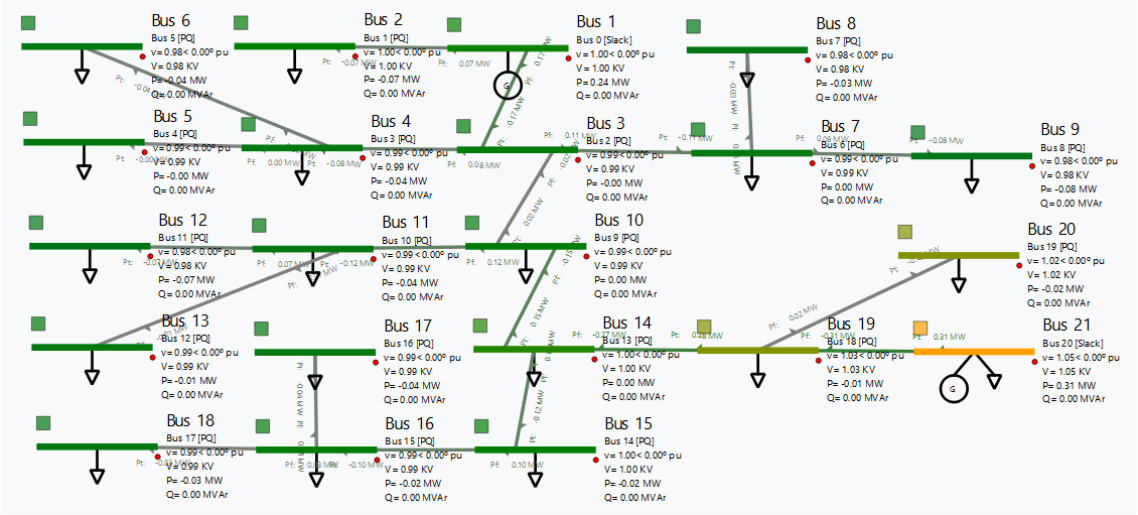

Figure 4: GridCal base case grid

4 Results Base case

The correct implementation of the power flow algorithms was verified, by comparing the calculated voltage profiles to the results in the paper [1]. In figure 7 it can be seen that the linear power flow approach shows significant deviations compared to the accurate solution (fsolve approach) but both profiles align with the one presented in the paper (figure 5 and in GridCal Figure 6).

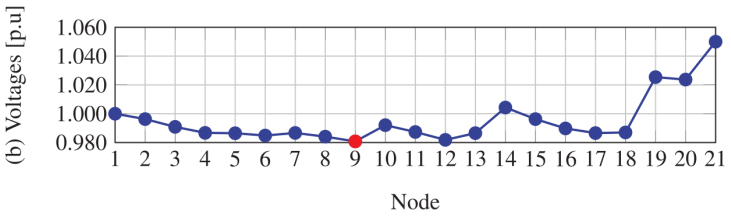

Figure 5: Voltage Profile as in [1]

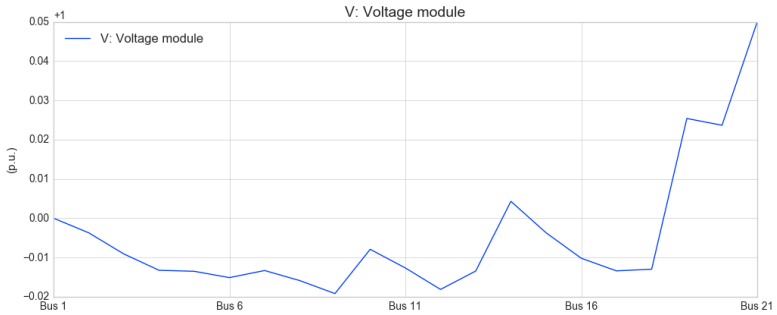

Figure 6: Voltage profile base case from GridCal

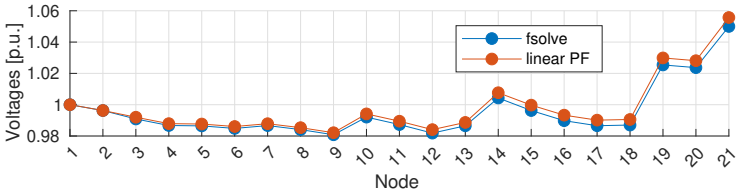

Figure 7: Voltage Profile Comparison

The exact values can be seen in table 3, it is noticed that the values from GridCal and from `fsolve` match perfectly. When comparing the linear power flow method and GridCal values it is seen a maximum voltage deviation of 0.00569 pu at bus 21. Since the linear power flow calculation was not performed with bus 21 as slack bus with 1.05 pu, but giving a discrete power input we can see deviations here. In general, the diviations are caused by the simplifications of the linear approach by eliminating the non-linear parts of the power flow equation ($V_i \sum \frac{V_i - V_j}{R_{ij}} = 1 \sum \frac{v_i - v_j}{R_{ij}}$).

	1	2	3	4	5	6	7	8	9	10	11	12	13	14	15	16	17	18	19	20	21
GridCal	1.00000	0.99628	0.99088	0.98672	0.98646	0.98486	0.98666	0.98409	0.98079	0.99207	0.98732	0.98185	0.98653	1.00429	0.99627	0.98979	0.98657	0.98700	1.02540	1.02368	1.05000
fsolve	1.00000	0.99628	0.99088	0.98672	0.98646	0.98486	0.98666	0.98409	0.98079	0.99207	0.98732	0.98185	0.98653	1.00429	0.99627	0.98979	0.98657	0.98700	1.02540	1.02368	1.05000
linear	1.00000	0.99629	0.99201	0.98790	0.98765	0.98607	0.98786	0.98533	0.98210	0.99412	0.98945	0.98408	0.98867	1.00765	0.99972	0.99332	0.99014	0.99056	1.02987	1.02811	1.05570
diff	0.00000	0.00001	0.00112	0.00118	0.00119	0.00121	0.00120	0.00124	0.00131	0.00206	0.00213	0.00223	0.00214	0.00335	0.00344	0.00352	0.00357	0.00356	0.00447	0.00443	0.00570

Table 3: Comparison of GridCal, fsolve and linear methods

For the following analysis, bus 21 is transformed from **slack** bus to a bus with **no generation**. This is done to have only bus 1 as a slack that acts as DC/AC connection to the transmission grid. With this setting, it is easy to determine if there is positive or negative power exchange of the DC microgrid with the AC network depending on the power balance of generation and load. At this point, it is already possible to show the extreme case where there is no (renewable) generation in the microgrid and the entire power is drawn from through the slack bus. The line between bus 1 and 3 is heavily loaded with a loss of $I^2R = 0.1283$ pu or 12.83% of the nominal voltage. This is far outside of the scope for typical losses around 5-10% and the positive-temperature-coefficient of copper (increase of resistance due to temperature rise) is not even considered. Additionally, the typical voltage operating band of ± 0.05 pu was violated as well (see figure 8).

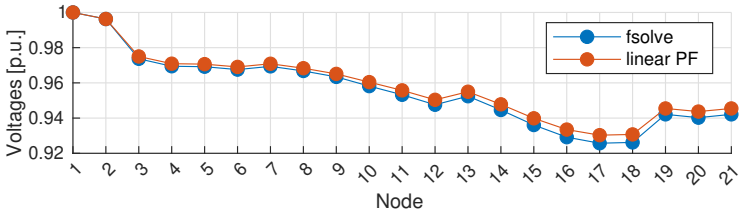

Figure 8: Voltage Profiles for Entire Generation by Slack Bus 1

5 Generation and Load Profiles

To accurately represent the temporal and spatial variability of demand in our DC microgrid test system, four distinct load profiles were implemented. These profiles

capture both industrial and residential consumption behaviors. The industrial profiles were derived from real-time SCADA data provided by industrial facilities, while the residential profiles are based on officially published standardized consumption curves provided by the Spanish Transmission System Operator (REE).

5.1 Industrial Load Profiles

Two industrial load types were selected from high-resolution datasets obtained directly from operational facilities:

- **Industrial Type 1: 'Rotoplas Plásticos'** – Nominal capacity of 5.3 MW.
- **Industrial Type 2: 'Marbran Congelados'** – Nominal capacity of 2.1 MW.

The measurements were recorded at 5-minute intervals across a full operating day and reflect the dynamic and process-dependent load profiles characteristic of manufacturing and cold storage operations. To isolate the relative temporal patterns from the absolute demand values, the time series were normalized into per-unit form. This normalized representation enables a scalable integration into the network model, where the load magnitude can be flexibly adjusted without distorting the inherent temporal dynamics.

Each industrial profile was replicated once, resulting in a total of four industrial loads distributed across the microgrid. These were strategically assigned to different buses to emulate geographic separation and load diversity while preserving technological type.

5.2 Residential Load Profiles

The residential demand was modeled using the official load profiles published by REE under the regulatory framework for 2025 (as per the resolution of December 23rd, 2024). These are standardized hourly profiles designed for tariff settlement purposes based on non-intrusive metering.

The selected profiles are:

- **Residential Type 1:** P2.0TD,0m,d,h – Representative of standard household consumption.
- **Residential Type 2:** P3.0TDVE,0m,d,h – Representative of households with EV charging infrastructure.

These profiles were extracted from the PERFF dataset (*Perfiles Finales de Consumo*) which aggregates and publishes demand curves derived from validated national measurements. The profiles reflect the typical behavior of residential consumers over a 24-hour cycle and are legally recognized for billing and balancing purposes.

5.3 Generation Profiles

To represent realistic distributed generation, two utility-scale photovoltaic (PV) generation profiles were integrated into the microgrid based on 5-minute SCADA data as well, from two operational plants:

- **Malvas I**: characterized by a stable daytime profile typical of clear-sky conditions.
- **San Miguel**: includes intermittent reductions in output due to modeled transient irradiance events.

The normalized curves were then scaled to nominal power outputs and assigned to four generation nodes in the network:

- **Nodes 5 and 9:** Profile of Malvas I (2.6 MW and 2.1 MW).
- **Nodes 12 and 18:** Profile of San Miguel (2.5 MW and 1.8 MW).

The incorporation of both ideal and perturbed PV generation profiles allows for comparative assessment of system performance under diverse solar conditions.

The complete set of profiles was embedded into the microgrid's nodal structure as constant power loads, allowing for detailed steady-state analysis under realistic and regulation-aligned operating conditions.

The internal DC microgrid generation was chosen to be purely solar, and each generation profile is assigned to 2 of the 4 generating units. Load profiles were evenly distributed.

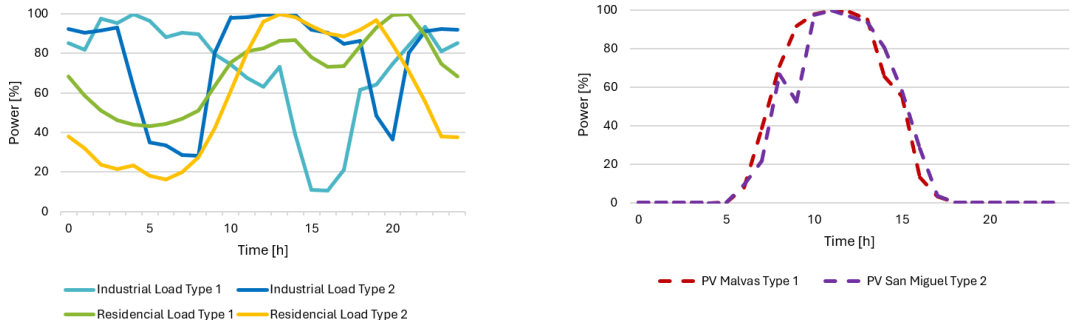

Figure 9: Load and Generation Time Series

5.4 Summary of Profile Sources and Characteristics

Category	Description	Source	Resolution
Industrial 1	Rotoplas Pl'asticos (5.3 MW)	SCADA measurements	5-min raw, 1h normalized
Industrial 2	Marbran Congelados (2.1 MW)	SCADA measurements	5-min raw, 1h normalized
Residential 1	Profile P2.0TD,0m,d,h	REE (PERFF 2025)	Hourly published data
Residential 2	Profile P3.0TDVE,0m,d,h	REE (PERFF 2025)	Hourly published data
PV Type 1	Malvas I (Stable Irradiance)	SCADA measurements	5-min raw, 1h normalized
PV Type 2	San Miguel (Variable irradiance)	SCADA measurements	5-min raw, 1h normalized

Table 4: Summary of Load Profiles Used in the Microgrid Model

5.5 Network Layout and Load/Generation Assignment

The diagram in Figure 10 illustrates the spatial distribution of loads and generation units across the 21-node DC microgrid. Based on the benchmark topology from the reference system, additional industrial and residential loads, as well as solar generation profiles, were strategically placed to replicate a realistic operational scenario.

Industrial Load Type 1 (plastics) and Type 2 (cold storage) were assigned to nodes 5, 4, 13, and 16, while residential loads of Type 1 (standard households) and Type 2 (with EV charging) were placed at nodes 8, 20, 11, and 19. Generation Profile Type 1, representing Malvas I, was assigned to nodes 5 and 9 with nominal capacities of 260 kW and 210 kW. Generation Profile Type 2, from San Miguel, was applied to nodes 12 and 18 with 250 kW and 180 kW, respectively.

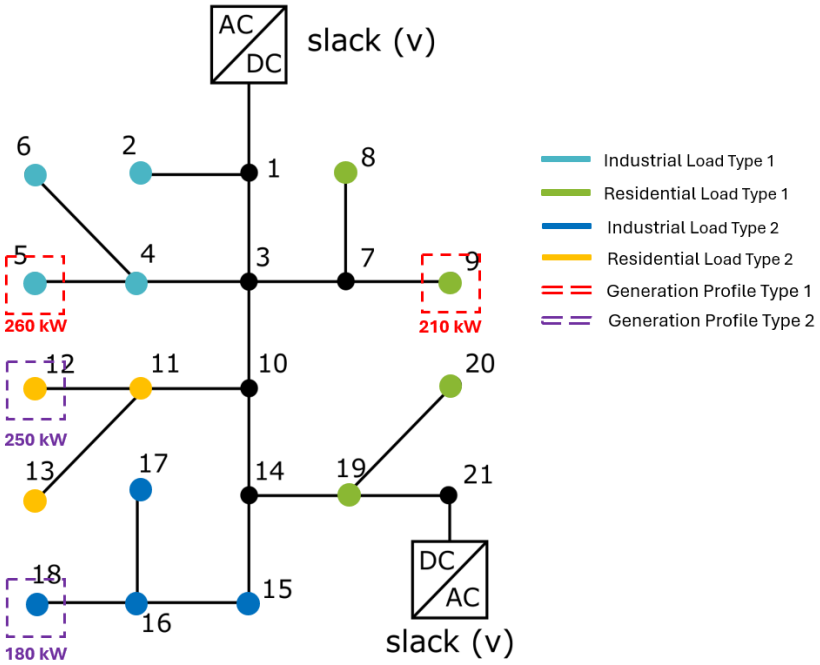

Figure 10: Node-level distribution of loads and generation units in the microgrid.

Node	Load [kW]	Load type
8	70	Residential 1
9	36	
19	4	
20	36	
11	45	Residential 2
12	68	
13	10	
2	70	Industrial 1
4	36	
5	4	
6	36	
15	22	Industrial 2
16	23	
17	43	
18	34	

Table 5: Node consumption assignment

Node	Generation [kW]	Profile
5	260	PV Malvas
9	210	
12	250	PV San Miguel
18	180	

Table 6: PV generation assigment

6 Time series results

This section analyzes the 24-hour dynamic operation of the DC microgrid under real-world demand and generation profiles, as introduced in Section 5. Based on Table 2 and Table 6, the total load reaches 5.33 p.u. and generation sums up to 9.0 p.u., creating an energy surplus that must be exported to the external AC grid.

Two operational scenarios are analyzed:

- **Scenario 1:** Dual connection to the main grid at buses 1 and 21.
- **Scenario 2:** Single connection at bus 1 only (bus 21 disconnected).

6.1 System Conditions and Power Flow Exchange

This surplus, calculated as 9.0 p.u. − 5.33 p.u. = 3.67 p.u., represents the amount of energy that must be exported to the AC grid.

Figure 11 shows the full-day power exchange between the DC microgrid and the main grid. Differences in behavior across the two scenarios highlight the impact of network redundancy.

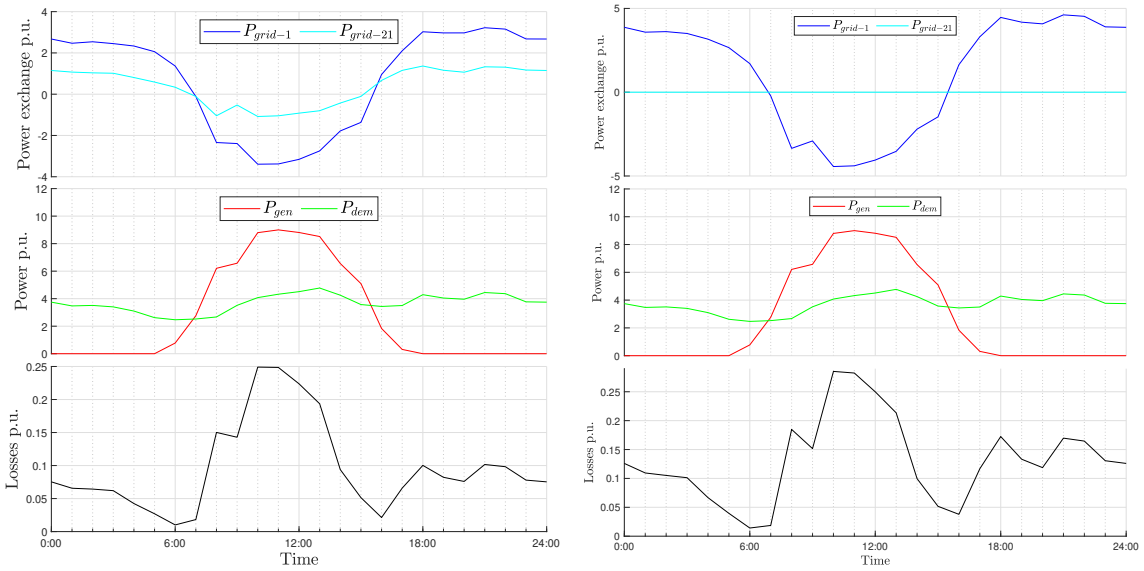

(a) Scenario 1 (b) Scenario 2

Figure 11: Power Flow Exchange

6.2 Grid Snapshots at Key Hours

Three representative time instants were selected for detailed inspection: 6:00 AM, 11:00 AM, and 9:00 PM.

6:00 AM – Low Load and Generation

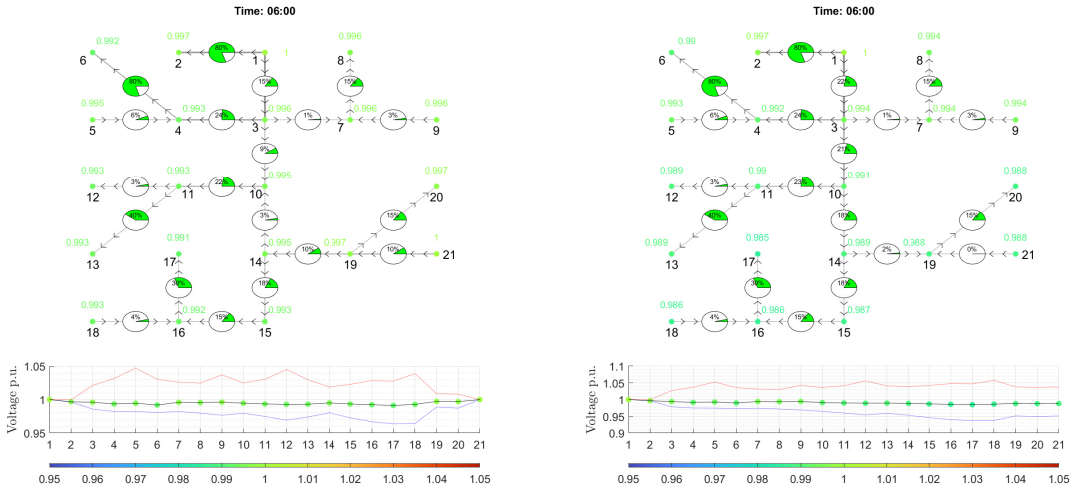

(a) Scenario 1 (b) Scenario 2

Figure 12: Network Conditions at 6:00 AM

At this time, both load and PV generation are minimal. Voltage profiles remain close to flat, with Scenario 2 presenting slightly more deviation due to reduced injection flexibility.

11:00 AM – Peak PV Generation

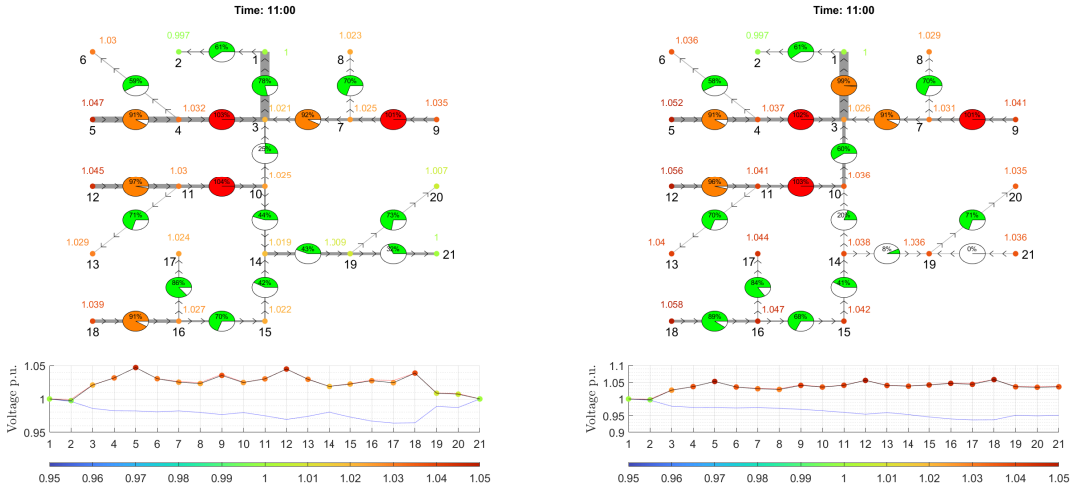

(a) Scenario 1 (b) Scenario 2

Figure 13: Network Conditions at 11:00 AM

This hour corresponds to maximum solar output. Scenario 1 efficiently evacuates the surplus, whereas Scenario 2 exhibits higher voltages at generation buses, stressing the grid.

9:00 PM – Peak Demand, No Generation

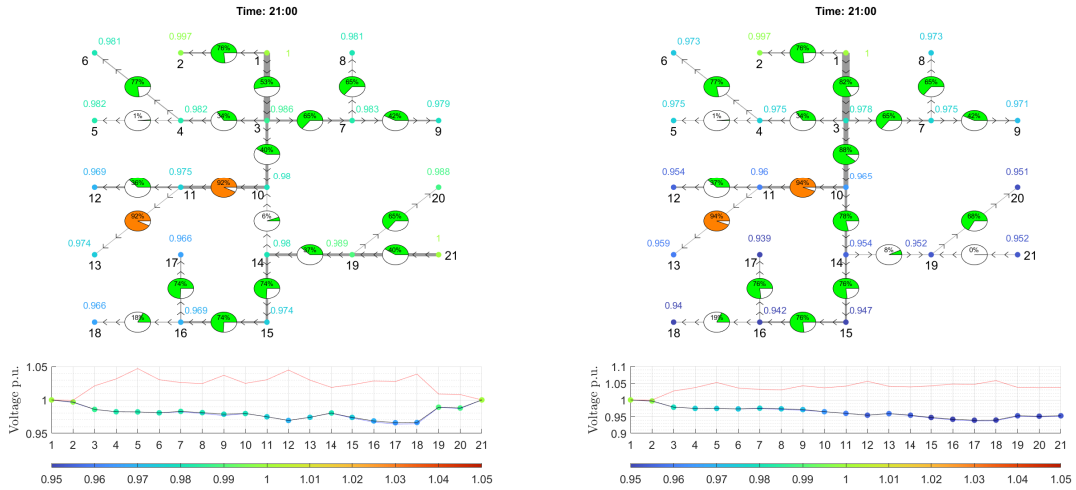

(a) Scenario 1 (b) Scenario 2

Figure 14: Network Conditions at 9:00 PM

With zero PV generation and peak demand, both scenarios import power. Scenario 2 shows deeper voltage sags due to limited feed-in.

6.3 GridCal Comparison – Heatmaps

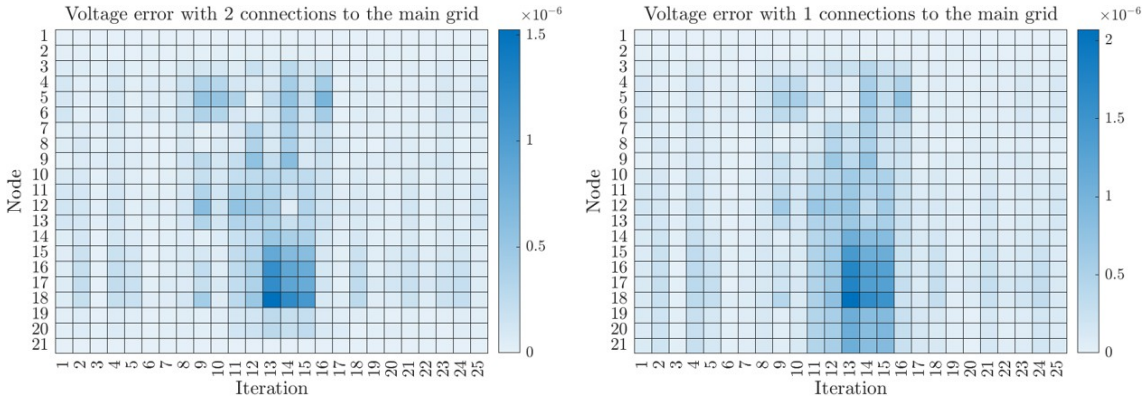

(a) Scenario 1 (b) Scenario 2

Figure 15: Voltage Error Heatmap

Numerical error between solvers remains below $2 \cdot 10^{-6}$ p.u., confirming model consistency. This confirms not only solver accuracy, but also the consistency between the independent MATLAB implementation and GridCal's numerical engine.

6.4 Performance Metrics Comparison

Metric	Scenario 1 (Dual)	Scenario 2 (Single)
Purchased Power (N1)	3.6890 MWh	5.2701 MWh
Delivered Power (N1)	2.0693 MWh	2.6563 MWh
Purchased Power (N21)	1.5237 MWh	-
Delivered Power (N21)	609.7 kWh	-
Maximum Current	391.2 A	514.3 A
Minimum Voltage	963.8 V	936.1 V
Maximum Voltage	1.047 kV	1.0628 kV
Power Losses	234.1 kWh	312.8 kWh

Table 7: Scenario Comparison Metrics

7 Conclusions

This report analyzed a 21-node DC microgrid under realistic industrial and residential demand patterns and variable PV generation. The system was tested under two configurations—single and dual connections to the AC grid—using both linear and nonlinear steady-state power flow methods.

This study demonstrated the operational advantages of implementing dual grid connections in a DC microgrid with high renewable penetration. Although a second point of connection entails higher infrastructure costs, these can be justified by long-term benefits such as reduced power losses (25%), improved voltage regulation, and a significant decrease in peak current magnitudes (24%). The dual-connection configuration enhances dispatch flexibility, distributes current flows more efficiently, and contributes to overall grid stability—factors that are particularly relevant for techno-economic assessments in microgrid design and planning.

The results also underscored the importance of effectively balancing local generation and consumption. During periods of solar surplus, the ability to export power becomes critical to avoid curtailment or costly redispatch operations. This reflects broader challenges in interconnected systems, where such limitations can incur significant costs.

For example, in Germany, transmission bottlenecks that trigger redispatch are financially compensated twice: renewable generators are remunerated for curtailed energy—even if it is not delivered—to safeguard investment returns. This can lead to paradoxical dynamics: Germany might pay Austria to absorb excess solar power into pumped hydro, only to later re-import power from Austria during demand peaks—effectively paying twice for energy that was never fully used nor produced at its origin.

Finally, it is important to note that this study assumes ideal generation forecasts and no contingencies. Future work should incorporate uncertainty modeling,

stochastic optimization, energy storage systems, and demand-side flexibility. These extensions would support more resilient planning and enable dynamic control strategies aligned with the evolution of modern DC grids.

8 Bibliography

[1] Danilo, O., et al. (2020). *Numerical methods for power flow analysis in DC networks: State of the art, methods and challenges*. Electrical Power and Energy Systems. https://doi.org/10.1016/j.ijepes.2020.106299

[2] Red Eléctrica (2024). *Redeia. Perfiles de consumo*. [Accessed 2025]. (TBD)

[3] Ministerio para la Transición Ecológica y el Reto Demográfico, España. (2024). *Resolución de 23 de diciembre de 2024, de la Dirección General de Política Energética y Minas, por la que se aprueba el perfil de consumo y el método de cálculo a efectos de liquidación de energía, aplicables para aquellos puntos de medida tipo 4 y tipo 5 de consumidores que no dispongan de registro horario de consumo, según el Real Decreto 1110/2007*.